

Thermal Evolution and Emission Properties of Strongly Magnetized Neutron Stars

Shubham Yadav,^{*} M. Mishra,[†] and Tapomoy Guha Sarkar[‡]

Department of Physics, Birla Institute of Technology and Science, Pilani, Rajasthan, India

Captain R. Singh[§]

Department of Physics, Indian Institute of Technology Indore, Simrol, Indore 453552, India

(Dated: December 14, 2023)

Emission properties of compact astrophysical objects such as Neutron Stars have been found to be associated with crucial astronomical observables. In the current work, we obtain the mass, pressure, and baryon number density profiles of the non-rotating neutron stars using the modified Tolman Oppenheimer Volkoff (TOV) system of equations in the presence of an intense radially distributed magnetic field. Employing the above profiles, we have determined the cooling rates of spherically symmetric neutron stars as a function of time with and without including the magnetic field using the NSCool code. We used a specific distance-dependent magnetic field in the modified TOV equations to obtain the profiles. We employ three different equations of states to solve the TOV equations by assuming the core of Neutron Stars to be made up of a hadronic matter. Using the above profiles, the cooling rate of neutron stars is obtained by employing the NSCool code. Furthermore, based on the cooling rate, we determine the luminosity of neutrinos, axions, and photons emitting from the neutron stars in the presence and absence of a magnetic field for different axion masses and three equations of states. Our comparative study indicates that the cooling rate and luminosities of neutrinos, axions, and photons change significantly due to the impact of the magnetic field.

PACS numbers:

I. INTRODUCTION

Neutron Stars (NSs) [1] are considered crucial observables as they allow the testing of physical theories at very high central matter density. Recent observations of gravitational wave events involving mergers of neutron stars have opened up new frontiers in the area of neutron star research [2–11]. There is also a renewed interest in studying neutron stars as they have been proposed to be the source of axionic dark matter particles. Several groups have suggested the possibility of detecting these axionic dark matter particles when they get converted to photons in the magnetosphere. The detailed study of neutron star physics is also crucial to make a comparative study with futuristic collider experiments like the Compressed Baryonic Matter Experiment (CBM) involving matter at very high density and low temperatures.

Recent investigations have revealed new information about the potency of magnetic fields inside and on the surface of compact objects [12–15]. The macroscopic structure, evolution, and observable astrophysical properties of neutron stars are strongly determined by the equation of state (EoS) of the matter and other sources in the energy-momentum tensor. Several observations such as, Soft Gamma Ray repeaters and X-ray pulsars

indicate that a specific group of neutron stars, called magnetars [16], possess a very strong magnetic fields. In the literature, it is established that the internal structure of neutron stars and their cooling properties get affected by the distribution of strong magnetic field in the interior [17, 18]. Magnetars are strongly magnetized neutron stars that exhibit a wide array of X-ray activity, with anticipated magnetic field intensities of up to 10^{18} Gauss [1]. This magnetic field is much larger than the level at which the electron's Landau level energies match its rest mass. In fact, the Virial theorem predicts the inner magnetic fields to be as high as 10^{18} Gauss. The exact origin of magnetic fields in different astrophysical objects is still an open area of research [19, 20]. Magnetars have attracted the attention of scientists due to their extraordinarily strong magnetic fields dependent properties [21]. This magnetic field may significantly modify the emission of high-energy electromagnetic radiation from these objects and thereby affect their cooling properties [4, 17, 19, 22–26].

A profile for the strength of the magnetic field [27] as a function of baryon chemical potential or matter density must be specified in order to analyze the impact of magnetic fields in the EoS of matter present inside the neutron stars. Instead, the nuclear physics research group developed and implemented ad-hoc magnetic field profiles [12–14]. They gave the following hypothesis to model a variable magnetic field that ascends toward the centers of the stars:

$$B(n_B/n_0) = B_{surf} + B_0 [1 - \exp[-\beta(n_B/n_0)^\gamma]], \quad (1)$$

where surface magnetic field is B_{surf} and maximum field

^{*}Electronic address: shubhamphy28@gmail.com

[†]Electronic address: madhukar@pilani.bits-pilani.ac.in

[‡]Electronic address: tapomoy@pilani.bits-pilani.ac.in

[§]Electronic address: captainriturajsingh@gmail.com

strength $B_{surf} + B_0$. The improved version of this model includes the baryon chemical potential and is used with model fit parameters $\beta = 0.01$ and $\gamma = 3$ [12]. They relate the magnetic field to the baryon number density in the star. Dexheimer et al. [13] present an accurate determination of the magnetic field profile inside a strongly magnetized neutron star. A quadratic polynomial (rather than an exponential function) simply depends on the selected values for the magnetic dipole moment and the baryon chemical potential as given by the equation:

$$B(\mu_B) = \frac{a + b\mu_B + c\mu_B^2}{B_c^2}\mu, \quad (2)$$

where μ_B is baryon chemical potential and μ is magnetic dipole moment, a and b are related to the properties of the star, like its mass.

Lopes et al. [28] has adopted a different way of introducing a variable magnetic field, which depends on the energy density rather than the baryonic density. This allows us to build a parameter-free model. Gomes et al. [29] shows the impact of powerful magnetic fields on the characteristics of hyperon stars. In order to study the structure of a neutron star in strong magnetic fields, Chatterjee et al. [30–32] presents a self-consistent model that takes into account general relativistic aspects as well as the influence of the magnetic field on the EoS, the interaction of the electromagnetic field with matter (magnetization), and anisotropies in the energy-momentum tensor. Chatterjee et al. [14] reported a thorough analysis of the magnetic field configurations in non-rotating neutron stars using an axisymmetric numerical code, altering the mass, the strength of the magnetic field, and the equation of state.

Several groups have attempted to compute the EoS of the matter contained inside the core of magnetars with and without considering finite baryon chemical potential [3, 12–14]. The study of magnetic field distribution as a function of distance, baryon chemical potential, rotation frequency, etc., has been presented in the Refs. [13, 14]. The effect of the magnetic field on the profile properties of the NS has been studied by Chatterjee et al., has studied magnetic field due to rotating magnetars by solving Einstein-Maxwell equations by modeling the current density in two different ways generated due to the rotation of the stars [1, 14, 33].

Apart from the magnetic field distribution in a neutron star [16, 34, 35], the EoS of matter under extreme conditions of very high density determines the internal structure and cooling properties of neutron stars [4, 17, 23, 31, 36, 37]. The EoS of hot and dense matter offers crucial knowledge regarding the properties of matter under these intense conditions. The composition of nuclear matter, its EoS, phase transitions, and condensates are all extensively examined in nuclear physics. Understanding various astronomical processes

associated with NSs and observations of gravitational wave signals presents a perfect opportunity to model several dense matter EoS models, particularly from the post-merger phase of binary neutron stars (BNS). Consequently, the study of hadronic matter's EoS in the presence of potent magnetic fields has come to light. The internal makeup of the stars and, consequently, the characteristics of dense matter significantly impact the macroscopic structure of neutron stars as well as their observable astronomical features. The EoS of Strongly magnetized neutron stars substantially affect their internal structure and macroscopic properties like mass and radius [3, 38, 39]. The stellar structure equations are obtained under the condition of hydrostatic equilibrium. Massive neutron stars may maintain equilibrium even in the presence of strong magnetic fields. However, for stable equilibrium, a neutron star must contain both poloidal (i.e., having only components B_r and B_θ) and toroidal (i.e., having only the azimuthal component B_ϕ) components since both are unstable on their own [31, 40, 41]. It is possible that such stars become unstable unless the toroidal and poloidal fields are both present and in some ratio [42]. Further, relativistic considerations of such highly magnetized neutron stars show that the magnetic energy decays on a timescale which is a function of the Alfvén crossing time and the rotation speed. It is relatively short compared to any evolutionary timescale [35, 43].

In the current work, we have investigated the impact of magnetic field on the pressure and mass profile of the non-rotating magnetars with mass $M \sim 1.4M_\odot$ employing three different microscopic model-based EoS, namely APR, FPS, and SLY. Magnetic field as a function of the distance from the center is calculated by using an eighth-order polynomial with a central magnetic field. The magnetic field thus obtained is used in a modified TOV system of equations to find the new pressure and mass profiles. We have determined the cooling rates of a few magnetars[44] as a function of time and EoS. We have studied the impact of a strong magnetic field on the cooling properties of such magnetars by obtaining the temperature as a function of distance from the center of the star at different EoS using the NSCool code [45]. On comparing our results with the corresponding calculations without a magnetic field, we find that the impact of a magnetic field must be addressed while performing precise calculations, especially for magnetars exhibiting a very high central magnetic field.

The paper is organized as follows. In Section I, we present the Introduction. In Section II, we describe the modified TOV equations, Equation of states, Neutron star cooling, and Axion physics. We have subsequently discussed the axion and neutrino emission rates. In Section III, we present the results and discussions on the impact of magnetic fields on various observables and macroscopic

NS properties. We have discussed how including a magnetic field affects the profile (mass, pressure) and cooling rates. Further, we investigate the luminosities (neutrinos, axions, and photons) for three axion masses. Finally, in Section IV, we summarize our results and conclude the work.

II. FORMALISM

A. TOV Equations for non-rotating neutron star

The present investigation is based on the modified TOV system of equations in the presence of a strong magnetic field. A profile for the strength of the magnetic field as a function of baryon chemical potential or density is required in order to analyze the impact of magnetic fields for a particular equation of the state of neutron stars. In Schwarzschild coordinates, the space-time metric inside the spherically symmetric star is given by:

$$ds^2 = -\exp(2\phi)c^2 dt^2 + \frac{dr^2}{1 - \frac{2Gm(r)}{rc^2}} + r^2 d\Omega, \quad (3)$$

where, $\exp(2\phi(R)) = 1 - \frac{2GM}{Rc^2}$.

The interior solution of Einstein's equation of General theory of relativity for this metric yields the following first-order differential equations (TOV) [46, 47]:

$$\frac{dm}{dr} = 4\pi r^2 \epsilon(r) \quad (4)$$

$$\frac{dP}{dr} = -\frac{G\left(\epsilon + \frac{P}{c^2}\right)(m(r)c^2 + 4\pi r^3 P)}{r(r c^2 - 2Gm(r))} \quad (5)$$

The above equations are to be integrated to obtain the pressure $P(r)$ and mass $m(r)$ inside the interior at a distance r under hydrostatic conditions. The boundary conditions for mass are $m(r=0) = 0$, $m(r=R) = M$. The core density is $\epsilon(r=0) = \epsilon_0$ and core pressure $P(r=0) = P_0$. The pressure decreases towards the surface, and at the radius, R of the star, the pressure $P(r=R)$ drops to zero [48]. The core pressure/mass can be obtained by solving these equations corresponding to the known central density and an equation of state.

Under the effect of the magnetic field, a magnetic energy density term is included in the matter density term of the TOV system of equations. The TOV equations undergo modifications when the magnetic field is present. Strong magnetic fields in magnetars will contribute as a source of the energy-momentum tensor and consequently affect the interior solutions. It has been shown that the TOV equations [47] may be modified by accounting for the contribution from the magnetic field to the energy density and a Lorentz force

term under the condition of hydrostatic equation [14].

The modified TOV equations in the presence of a magnetic field are given by:

$$\frac{dm}{dr} = 4\pi r^2 \left(\epsilon + \frac{B^2}{\mu_0 c^2} \right) \quad (6)$$

$$\frac{d\phi}{dr} = \frac{G(m(r) + 4\pi r^3 P/c^2)}{r(r c^2 - 2Gm(r))} \quad (7)$$

$$\frac{dP}{dr} = -c^2 \left(\epsilon + \frac{B^2}{\mu_0 c^2} + \frac{P}{c^2} \right) \left(\frac{d\phi}{dr} - \mathcal{L}(r) \right), \quad (8)$$

where $\mathcal{L}(r)$ denotes a Lorentz force contribution [14]. The distribution of the magnetic field in the interior of the star shall affect the mass and pressure profiles. Assuming azimuthal symmetry the magnitude of the magnetic field $B = (\vec{B} \cdot \vec{B})^{1/2}$ is generally expressible as a sum:

$$B(r, \theta) \approx \sum_{l=0}^{l_{max}} B_l(r) Y_l^0(\theta). \quad (9)$$

It has been seen using simulations [48] that the monopole term dominates significantly over the others. We shall ignore the anisotropies as a first approximation in our work. We emphasize that the vector magnetic field B cannot have a monopole component. The "monopole" here refers to the norm of the magnetic field. We also recognize that stability analysis of the neutron stars in the presence of strong magnetic fields would naturally require the presence of toroidal and poloidal fields[42]. In principle, it has been shown that the toroidal fields can be much stronger for realistic stars than the poloidal fields [41, 42]. We have adopted a simplified pure radial profile for the monopolar term of B (it must be noted that we are not looking at magnetic monopoles here) as a polynomial fit function obtained in [49, 50] given by:

$$B_0(r) = B_c \left[1 - 1.6 \left(\frac{r}{\bar{r}} \right)^2 - \left(\frac{r}{\bar{r}} \right)^4 + 4.2 \left(\frac{r}{\bar{r}} \right)^6 - 2.4 \left(\frac{r}{\bar{r}} \right)^8 \right], \quad (10)$$

where \bar{r} is the star's mean radius. Finding a suitable radius because of star distortion due to a magnetic field is challenging. Therefore, the mean radius \bar{r} is directly related to the star's surface and emission properties. We note that the mean radius \bar{r} is not much sensitive to the magnetic field, which may nevertheless cause distortions in the profile. From the graph, we determined the mean radius (\bar{r}) at a fixed central magnetic field value. We have adopted a fiducial value of $B_c = 10^{18}G$ in our analysis. We have used this as an universal magnetic field profile and neglected the possible variations that may arise from different EoSs.

The phenomenological modeling of the effect of the magnetic field [36] is used to write an effective Lorentz force term in the modified TOV equations as [14];

$$\frac{\mathcal{L}(r)}{10^{-41}} = B_c^2 \left[-3.8 \left(\frac{r}{\tilde{r}} \right) + 8.1 \left(\frac{r}{\tilde{r}} \right)^3 - 1.6 \left(\frac{r}{\tilde{r}} \right)^5 - 2.3 \left(\frac{r}{\tilde{r}} \right)^7 \right] \quad (11)$$

B. Equation of State

In the current work, APR, FPS, and SLY EoSs are considered to study the thermodynamic behavior of the NS's interior. In Akmal-Pandharipande-Ravenhall (APR) [51, 52], EoS interaction potential is parameterized using baryon density and isospin asymmetry [53, 54]. APR EoS shows the transition between the low-density phase (LDP) to the high-density phase (HDP). Nucleons are the constituent in LDP, while HDP corresponds to a spin-isospin-ordered neutral pion condensate. It is also observed that phase transition in the APR EoS speeds up the star's shrink rate. The FPS EoS gives a unified description of the inner crust and the liquid core. In this model, the crust-liquid core transition takes place at higher density $\rho_{edge} = 1.6 \times 10^{14}$ gm/cm³ and is preceded by a sequence of phase transitions between various nuclear shapes. The sequence of phase transitions starts when cylindrical ones replace spherical nuclei immersed in neutron gas. All phase transitions are very weakly first-order, with relative density jumps smaller than 1%. The SLY EoS describes the cooling near the minimum mass of the solid crust and liquid core consistently. The SLY EoS of neutron star matter is based on the SLY effective nuclear interaction model. In this model, nuclei in the ground state of neutron star matter remain spherical down to the bottom edge of the inner crust. Transition to the uniform ionized matter (npe) plasma occurs at $\rho = 1.3 \times 10^{14}$ g/cm³. The crust-core phase transition is very weakly first-order, with a relative density jump of about 1%. The SLY arises due to the unique properties of neutron stars. The characteristics of neutron stars [55] close to M_{min} are determined by the EoS of dense matter at subnuclear densities, particularly in the density interval $0.1\rho_0 < \rho < \rho_0$. At such densities, the actual structure of the ground state of matter results from the interplay of the surface and Coulomb terms in the total energy density. These tiny "finite size" terms, absent in uniform npe matter, are difficult to calculate with high precision at the thickness of interest. However, being very small compared to the main bulk energy contribution, these terms decide the actual shape of nuclei and whether matter with nuclear structures is energetically preferred over the spatially npe. It is mandatory to use the same effective nuclear Hamiltonian to describe nuclear structures (nuclei) and neutron gas inside the inner crust and the uniform npe matter of the liquid core. For non-spherical nuclear shapes in the bottom layers of the inner crust depends on the assumed model of the effective

nuclear Hamiltonian. In the case of a different effective nuclear Hamiltonian, FPS EoS is the most suitable [56]. In the vicinity of the crust-core interface, the SLY EoS is stiffer than the FPS one. Moreover, in the case of the SLY EoS, the discontinuous stiffening at the crust-core transition is more pronounced than in the FPS case, where it has been preceded by a sequence of phase transitions connected with changes in nuclear shapes. Such a sequence of phase transitions implied a gradual stiffening of matter.

C. Neutron star cooling

Neutrino emission is the dominant process that causes neutron star cooling [57–60] at early times and high temperatures. The NSCool is a FORTRAN-based, neutron star cooling computational program [45]. This package also includes several pre-built stars, many EoSs to build stars, and a TOV integrator to build stars from an EoS. The algorithm solves the heat transport and energy balance equations in full GR once pressure, density, and mass profiles are given after solving the TOV equations for a particular Star. Assuming the star interior is isothermal and neglecting GR effects, and by focusing only on the energy conservation equation, one can have a reasonable understanding of the fundamental characteristics of neutron star cooling [4, 17, 19, 22, 23, 61–63]. The corresponding equation following Newtonian formulation is as follows [64]:

$$C_v \frac{dT_b^\infty}{dt} = -L_\nu^\infty - L_a^\infty - L_\gamma^\infty(T_s) + H, \quad (12)$$

where C_v total specific heat, L_ν^∞ is the energy sinks are the total neutrino luminosity, L_a^∞ is the axion luminosity, L_γ^∞ is surface photon luminosity, H includes all possible heating mechanisms, T_s is the surface temperature and T_b^∞ internal temperature. $L_\gamma^\infty = 4\pi\sigma R^2(T_s^\infty)^4$, with σ as Stefan-Boltzmann's constant and R is the radius of the star. $T_s^\infty = T_s \sqrt{1 - 2GM/c^2R}$. Here infinity superscript indicates that the external observer is at infinity and measures these quantities on the redshifted scale. Typically, $T_s^\infty/T_s \sim 0.7$. The cooling profile in the inner layers of the neutron star obtained from Eq.(12) gives a simplistic isothermal model of thermal evolution. Generalizations involving multidimensional heat transport equation [24] may provide more realistic results for NS ages $t < 100$ yrs. One may obtain approximate scaling laws for the cooling process whereby the effective temperature T_e scales with time as $T_e \sim t^\nu$. The exponent $\nu = -1/12$ and $\nu = -1/8$ for slow and fast neutrino cooling, respectively. Here we assume $H = 0$ and superfluidity in the entire neutron star cooling. Assuming the thermal relaxation time scale of the envelope is shorter than the stellar evolution time scale, and there is minimal neutrino emission within the envelope. In that case, heat transport and hydrostatic equilibrium can be reduced to

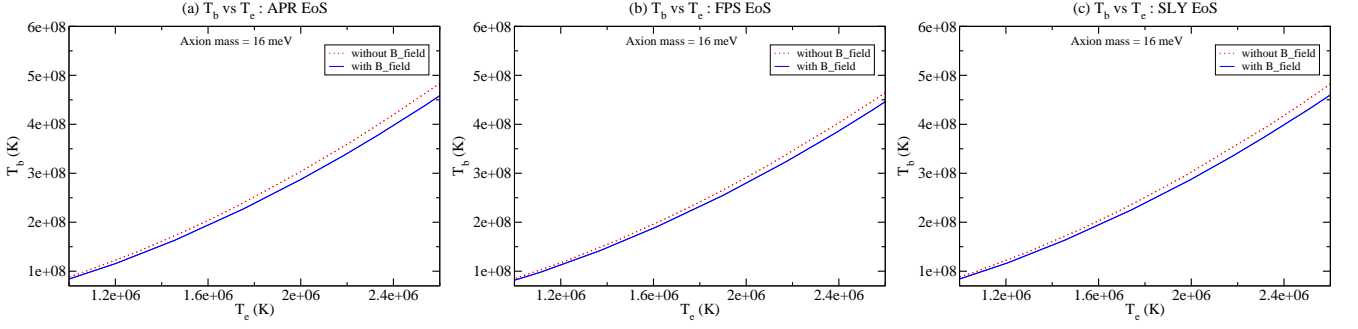


FIG. 1: The variation of effective surface temperature T_e with temperature T_b for three different EoS in the presence and absence of magnetic field

ordinary differential equations. These equations can be easily solved, provided they have the correct physical input. The surface temperature $T_s \equiv T_e$ is the outcome for every given $T_b \equiv T(\rho_b)$. Typically, it's referred to as a $T_b - T_s$ or $T_b - T_e$ relationship. The presence of a magnetic field that modifies the TOV equations manifests significantly on the $T_b - T_e$ relationship calculated using NSCool code [45] as seen from the Figure (1). The variation of the observed temperature T_e with the internal temperature T_b is shown in Figure (1). The $T_b - T_e$ curves show that at a fixed value T_b , the surface temperature T_e in the presence of a strong magnetic field is higher than T_e in the absence of the magnetic field [65]. The monotonic rise of T_e with T_b is similar to the behavior reported earlier by [64]. The $T_b - T_e$ relationship has been estimated in many previous works [66–68]. Considering a very intense magnetic field in hot blanketing envelopes of neutron stars, the structure of HBEs may be affected by enhanced neutrino emission [65, 69–73]. The boundary of the heat blanketing envelopes (HBEs) is ϵ_b ($\rho_b \sim 10^{10}$ gm/cm³). The magnitude of the magnetic field at HBEs is taken as 10^{13} Gauss and it has a radial dependence given by Eq.(10). The HBEs contain either iron or successive layers of hydrogen, helium, carbon and iron. The radiative opacity for a fully ionized, non-relativistic, and non-degenerate plasma, composed of electrons and ions is determined by the Kramers' formula given by: [74]:

$$K_r(0) = 75\bar{g}_{eff} \left(\frac{Z^3}{A^2} \right) \rho \left(\frac{10^6 K}{T} \right)^{3.5}, \quad (13)$$

where A and Z are relative atomic weight and mass number, respectively, and $\bar{g}_{eff} \sim 1$ is the effective Gaunt factor, ρ is measured in gm/cm³. The strong magnetic fields affects the thermal conduction in the outer layers of the NS, thereby affecting heat flows near the stellar surface and the effective surface temperature. The relation between radiative opacities arising from free-free transitions is given by [74]:

$$K_r(B) = 2.2\bar{g}_{eff} Z^3 \rho A^{-2} \left(\frac{10^6 K}{T} \right)^{1.5} \left(\frac{10^{12} G}{B} \right)^2, \quad (14)$$

where $\bar{g}_{eff} \sim 1$ is the effective Gaunt factor and ρ is measured in gm/cm³. We note that though the radiative conductivity becomes anisotropic in the presence of strong magnetic fields. We have neglected the difference between the longitudinal and transverse components in our work.

Nevertheless, a magnetic field inside the heat blanketing layer of neutron star can strongly affects the electron thermal conductivity. Here we consider only thermal conductivity of electrons which becomes a tensor quantity (with three non-zero components) in the presence of a magnetic field. The three thermal conductivities coefficients are given by parallel (κ_{\parallel}) and transverse κ_{\perp} to the field and hall κ_H which describes component perpendicular to B and temperature gradient. The effective electron thermal conductivity is given by [69, 74, 75]:

$$\kappa = \kappa_{\parallel} \cos^2 \theta_B + \kappa_{\perp} \sin^2 \theta_B, \quad (15)$$

where

$$\kappa_{\parallel} = \frac{\pi^2 k_B^2 T n_e \tau_e}{3m_e^*}, \quad (16)$$

In the above equation, τ_e is the effective electron thermal-conduction relaxation time and n_e is the electron number density.

$$\kappa_{\perp} = \frac{\kappa_{\parallel}}{1 + (\omega^* \tau_e)^2}, \quad (17)$$

where $\omega^* = \omega_c / \gamma_r$, with $\omega_c = eB/m_e c$, $\gamma_r = \sqrt{1 + x_r^2}$ and $x_r = \frac{p_F}{m_e c}$. Finally, the product $\omega^* \tau_e = 1760 \left(\frac{B_{12}}{\gamma_r} \right) \left(\frac{\tau_e}{10^{-16} s} \right)$, with $B_{12} = B/10^{12}$ Gauss. Here θ_B is the angle between the direction of magnetic field and normal to the surface.

D. Axions

The axions are pseudo-Nambu-Goldstone boson [76–81] emerging as dark matter particles. These are motivated by the Peccei-Quinn solution to the strong-CP problem in which a theta term in QCD Lagrangian is

canceled by introducing a scalar field (the so-called QCD Axions) [82–84]. Due to astrophysical and cosmological constraints, axions must have rest mass $m_a \sim 10^{-6}$ eV to 10^{-2} eV [85–89]. Recently, it was reported that axions thermalize to form a Bose-Einstein condensate (BEC), which differs from ordinary cold dark matter (CDM) in the non-linear regime of structure formation. In order to study the production of DM Axions, we need NS cooling [90, 91]. There is continuous heat transport from the interior of NS to the surface. These very light particles [92] may be emitted from the interiors or the surface of the neutron stars. In fact, axions in an extended NSs magnetospheres [93] can couple to virtual photons and produce the real photons due to Primakoff effect [94, 95]. As per the current status of experimental searches for the distribution of dark matter, it can be concluded that axions may remain an excellent dark matter candidate for future experiments. The Axionic Dark Matter experiment, (ADMX) [96, 97] will cover a large fraction of the axion parameter space. According to the ADMX experiment, if these very light particles exist, then it could be possible that they would decay into pair of light particles, thus making them difficult to detect [92, 97, 98]. There are two axion models; the Dean-Fischler-Srednitsky-Zhitnitsky - DFSZ model [99, 100], which includes an additional axion coupling to the charged leptons, while the Kim-Shifman-Weinstein-Zakharov (hadronic) - KSVZ model restricts the Axion's interactions to photons and hadrons. In our current work, we have followed the KSVZ axion model. It is extensively addressed in the overview of Axion physics, how axion phenomenology relates to various astrophysical processes.

E. Neutrino-Axion emission inside NS core

1. Cooper Pair Breaking and Formation process (PBF)

Microscopic theories of dense matter play a crucial role in cooling compact stars and investigating the composition of the inner core. Both the neutrino and photon emissions are controlled by the supranuclear densities and the structure of the stellar outer layers [90, 101–103], respectively. The concept of pairing provides new pathways for neutrino emission in addition to well-known suppressing effects on the specific heat and neutrino emissivities. The low value of Fermi momenta, particularly for nucleon pairing, is predicted to occur in the 1S_0 angular momentum state. This happens at densities corresponding to the outermost part of the core. Mainly, it appears at densities of the outer core where only protons are minimally mixed with neutrons, making the pairing process more sensitive. Cooper pairs are expected to form and break when the superfluid condensate is in thermal equilibrium with the broken pairs. This usually happens at a temperature far below superfluid critical temperature T_c . Neutrino and Axion can be produced due to the for-

mation of a Cooper pair liberating energy which can be taken away by a $\nu\bar{\nu}$ pairs.

$$\begin{aligned} n + n &\rightarrow [nn] + \nu + \bar{\nu} \\ p + p &\rightarrow [pp] + \nu + \bar{\nu} \end{aligned}$$

In the current work, we have not included the neutrino emission processes namely, the direct and modified Urca processes.

Neutrino emission rate

The substantial cooling of NSs with superfluid inside the core by emitting neutrinos through Cooper pair-breaking processes (PBF) [90, 99, 101, 102, 104] is driven by axial-vector currents when the temperature [105–107] lies below the critical temperature $T_c = 10^9$ K. For neutron/proton 1S_0 -wave paired superfluid, the emissivity [103, 104, 108] of neutrino is given by:

$$\epsilon_\nu^s = \frac{5 G_F^2}{14\pi^3} v_N(0) v_F(N)^2 T^7 I_\nu^s. \quad (18)$$

Here the integral I_ν^s is;

$$I_\nu^s = z_N^7 \left(\int_1^\infty \frac{y^5}{\sqrt{y^2 - 1}} [f_F(z_N y)]^2 dy \right), \quad (19)$$

where ϵ_ν^s is neutrino emissivity and G_F is Fermi's coupling constant $= 1.166 \times 10^{-5} \text{GeV}^{-2}$. $z = \Delta(T)/T$ with $\Delta(T) = 3.06 T_c \sqrt{1 - \frac{T}{T_c}}$. Here T_c is the critical temperature for neutron/proton superfluid. The neutrino emissivity due to the P-wave paired neutron superfluid is taken from ref. [101].

Axion emission rate

In this section, we briefly describe the axion emission rate inside NSs core [93, 109] from Cooper pair breaking and formation process (PBF) [99] process. In order to calculate the production rates in the NSs core, prerequisites are the temperature profiles in the core, the metric, the critical temperature profiles, neutron and proton Fermi's momenta profile (which depends on the equation of state). The modified TOV system of equations (in the presence of magnetic field and their counterparts) profiles are used after making specific changes (to include axion emission) in the NSCool code to determine the cooling rate and luminosities. Both spin-0 S-wave and spin 1 P-wave nucleon superfluids could exist inside the NS core. The axion emission rate [90, 99] due to the neutron S-wave pairing from the Cooper pair-breaking formation (PBF) [104] is given by:

$$\epsilon_a^s = \frac{8}{3\pi f_a^2} v_n(0) v_F(n)^2 T^5 I_a^s. \quad (20)$$

The integral I_a^s is expressed as:

$$I_a^s = z_n^5 \left(\int_1^\infty \frac{y^3}{\sqrt{y^2-1}} [f_F(z_n y)]^2 dy \right), \quad (21)$$

where ϵ_a^s is axion emissivity, f_a is axion decay constant, $v_n(0)$ density of state at Fermi surface and $v_F(n)$ is fermi velocity of neutron.

$$v_n(0) = \frac{m_n p_F(n)}{\pi^2} \quad (22)$$

$$z = \frac{\Delta(T)}{T}, \quad (23)$$

$$f_F(x) = [e^x + 1]^{-1}, \quad (24)$$

with $x = \frac{\omega}{2T}$, where ω is the axion energy.

The ratio of axion and neutrino emissivities is given by:

$$\epsilon_a^s = \left(\frac{59.2}{f_a^2 G_F^2 [\Delta(T)]^2} r(z) \right) \epsilon_\nu^s, \quad (25)$$

where,

$$\Delta(T) \simeq 3.06 T_{cn} \sqrt{1 - \frac{T}{T_{cn}}}. \quad (26)$$

The numerical values of the $r(z) = z^2 I_a^s / I_\nu^s$ associated with axion and neutrino emissivity integrals for the different values of z around one are always less than unity.

$$f_a > 5.92 \times 10^9 \text{ GeV} \left[\frac{0.1 \text{ MeV}}{\Delta(T)} \right]. \quad (27)$$

Here f_a is a axion model-dependent variable [64]. Axion mass m_a is related to f_a by the equation; [99, 100, 110, 111]:

$$m_a = 0.60 \text{ eV} \times \frac{10^7 \text{ GeV}}{f_a}. \quad (28)$$

Here, we have assumed the axion emissivity due to proton S-wave pairing [99, 112, 113] will remain the same as axion due to neutron S-wave pairing provided $C_n = C_p$ and $T_{cn} = T_{cp}$, where T_{cn} and T_{cp} are critical temperatures for neutron superfluid and proton superfluid, respectively.

The axion emissivity due to the P-wave paired neutron superfluid is given by [99]:

$$\epsilon_a^P = \frac{2 C_n^2}{3\pi f_a^2} v_n(0) T^5 I_a^P, \quad (29)$$

where C_n is the axion model dependent constant.

The integral I_a^P is expressed as:

$$I_a^P = z_n^5 \left(\int_1^\infty \frac{y^3}{\sqrt{y^2-1}} [f_F(z_n y)]^2 dy \right), \quad (30)$$

where $z_n = \Delta^P(T, \theta)/T$ with θ is the polar angle. There exist two states of P-wave superfluid pairing denoted as A and B expressed as:

$$\Delta_P^A = \Delta_0^A \sqrt{1 + 3 \cos^2 \theta}. \quad (31)$$

and

$$\Delta_P^B = \Delta_0^B \sin \theta. \quad (32)$$

F. Neutrino-Axion emission inside NS crust

1. e-e Bremsstrahlung process

Neutrino emission rate

The neutrino emission rate for e-e Bremsstrahlung process is given by [99, 109]:

$$\epsilon_{\nu ee, \text{brem}} = 7.42 \times 10^{-2} G_F^2 Z^2 \alpha_e^4 n_i T^6 L. \quad (33)$$

Here n_i is nuclei number density, $\alpha_e = 1/137$ is the QED fine structure constant, and L incorporates many-body corrections to process rate related to nuclei correlations.

Axion emission rate

The NSs crust may emit axions when a degenerate relativistic electron strikes an ion with charge Z and mass number A . The axion emission rate is given by [99, 109]:

$$\epsilon_{aee, \text{brem}} = \frac{\pi^2}{120} \frac{Z^2 \alpha_e}{A} \left(\frac{g_{aee}}{\epsilon_F} \right)^2 n_B T^4 \left[2 \ln(2\gamma) - \ln \frac{\alpha_e}{\pi} \right]. \quad (34)$$

Here g_{aee} is coupling of axions to electrons, $g_{aee} = \frac{C_e m_e}{f_a}$, γ is the Lorentz factor of electrons, ϵ_F is the electron's fermi energy, n_B is baryon number density, and $\alpha_e = 1/137$ is the QED fine structure constant. By making electron PQ charge $C_e=1$, $L=1$ and $\frac{m_e}{\epsilon_F} = 10^{-2}$ the relation between Axion to neutrino emissivity is given by:

$$\epsilon_{aee, \text{brem}} = \left[2.8 \left(\frac{10^9 K}{T} \right)^2 \left(\frac{10^{10} \text{ GeV}}{f_a} \right)^2 \right] \epsilon_{\nu ee, \text{brem}}. \quad (35)$$

We want to emphasize here that we have not considered the influence of strong fields on the mentioned neutrino and axion cooling mechanisms.

III. RESULTS AND DISCUSSIONS

Figure (2) depicts the variation of mass with respect to the distance from the center of the NS for three different EoSs, namely APR, FPS, and SLY, in the presence of the magnetic field. It indicates that the variation of mass $m(r)$ as a function of distance from the center of the NS change little due to the effect of the magnetic field. The difference is seen at some intermediate radial distances. The APR, FPS, and SLY models show an approximately 16.7%, 15.4% and 17.5% departure from the corresponding results without including magnetic field $r \sim 4500$ m, respectively.

Figure (3) shows the variation of pressure as a function of distance from the center of the NS for three different EoSs, namely APR, FPS, and SLY, before and after taking into account the magnetic field. Here a

significant difference due to the magnetic field is seen. The departure from the case with the magnetic field increases with the radial distance from the center. After incorporating the magnetic field, the $P(r)$ curve lies above the corresponding curve without the magnetic field effect and the curves coincide at $r \sim 8100$ m for APR and SLY model EoSs, and $r \sim 7400$ m for FPS model EoS. On comparing the slope of the two curves, it is found that the pressure decreases slower after including the magnetic field. The behavior for three different EoSs is qualitatively similar, and the APR, FPS, and SLY models show an approximately 20.1%, 18.5% and 20.2% departure with respect to the case of with magnetic field at $r \sim 4500$ m, respectively. The imprint of the magnetic field on the cooling properties of the neutron star is studied using the NSCool code [45].

<i>EoS</i>	R (without B field) (km)	R (with B field) (km)
APR	11.77	10.37
FPS	10.79	9.68
SLY	11.64	10.43

TABLE I: Table showing radius (R) of NSs corresponding to the mass $M = 1.4M_{\odot}$ for different EoS.

In Figure (4), we first look at the temperature profile for axion mass ~ 16 meV as a function of radial distance from the center at a particular time corresponding to a characteristic age of a particular NS for the APR EoS. The same is shown for two more NSs having two different characteristic age with axion mass ~ 16 meV. The characteristic age used here are 9.7×10^2 yrs [31, 114], 3.3×10^4 yrs [115, 116] and 7.3×10^3 yrs [117, 118] for the three figures in the panel, respectively. From the figures, it is clear that in the presence of a magnetic field, the cooling property of the star undergoes a considerable change. As the star cools, in the absence of the magnetic field, the temperature remains lesser than the case when there is magnetic field at all distances and at all times.

For a given star, the presence of a strong magnetic field and an associated high magnetic field energy lead to a decrease of thermal energy while the gravitational energy remains unchanged. This explains the correlation between the suppression of luminosity and the strength

of the magnetic field. Similar suppression of temperature in white dwarf stars with magnetic fields is reported in earlier works [36]. The strong magnetic field may affect the EoS and may also cause sizable changes to thermal conduction and observable properties. We have not incorporated the impact of magnetic field on the EoS in the current work.

Figure (5) and Figure (6) show the temperature as a function of the radius for the characteristic age of three NSs for FPS and SLY EoS, respectively. While the FPS EoS does not show any qualitatively different behavior from the APR EoS, the departure of the temperatures from the no-magnetic field case is always higher. The SLY EoS also indicates no qualitative changes in the temperature profile, and $T(r)$ at all radial distances remains higher than their counterpart in the no-magnetic field case at all times. At larger times for this EoS, the temperature departure is higher than in the no-magnetic field. Table II shown below summarises the results.

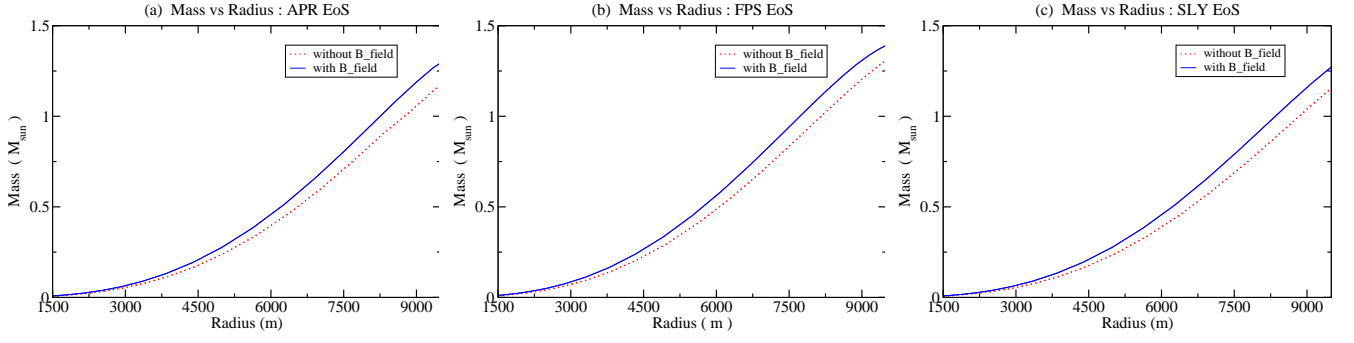


FIG. 2: The variation of mass with radial distance r for three different EoS in the presence and absence of magnetic field.

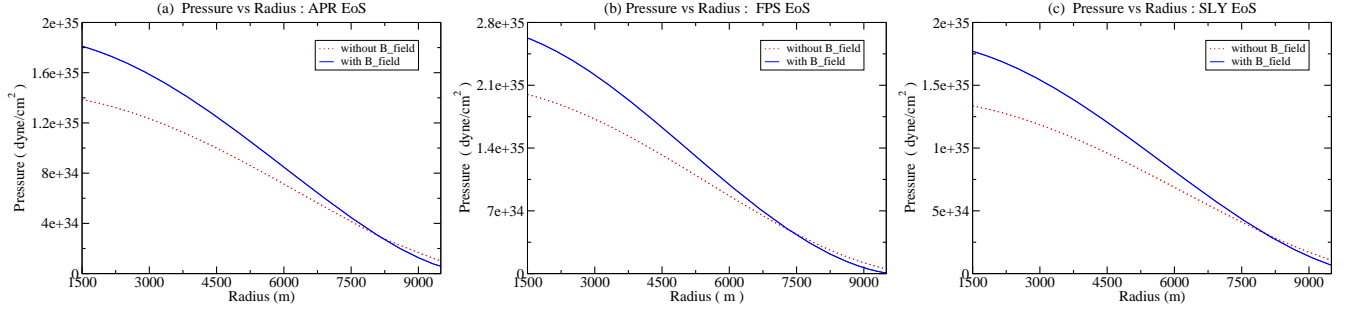


FIG. 3: The variation of pressure with radial distance r for three different EoS in the presence and absence of magnetic field.

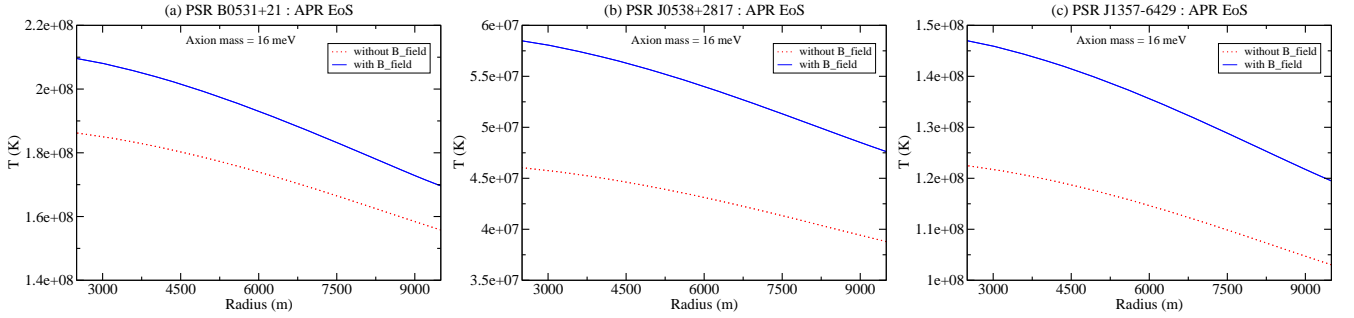


FIG. 4: The variation of temperature with radial distance r for three different Neutron Stars for APR EoS in the presence and absence of magnetic field.

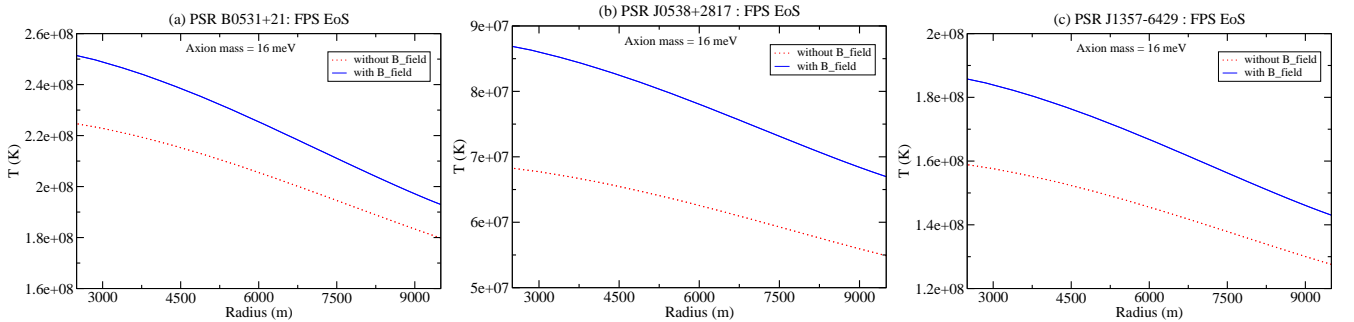


FIG. 5: The variation of temperature with radial distance r for three different Neutron Stars for FPS EoS in the presence and absence of magnetic field.

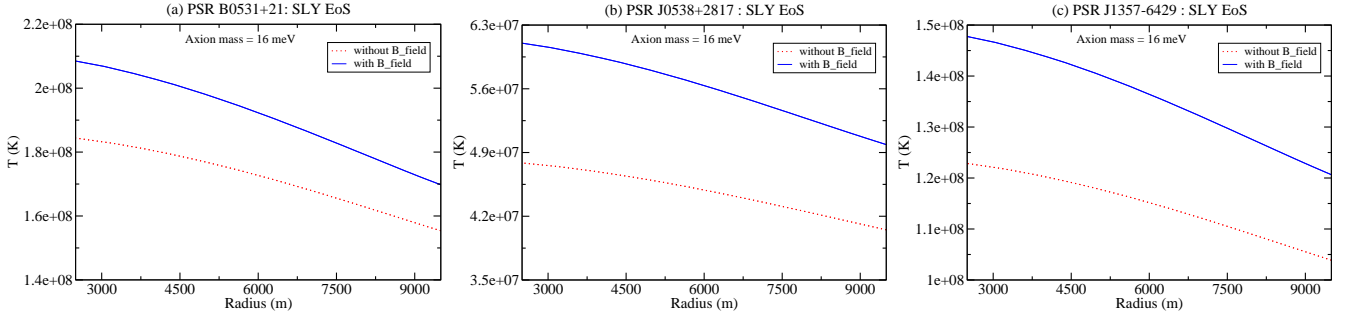


FIG. 6: The variation of temperature with radial distance r for three different Neutron Stars for SLY EoS in the presence and absence of magnetic field.

$m_a = 0.016$ eV	Age = 9.7×10^2 yrs	Age = 3.3×10^4 yrs	Age = 7.3×10^3 yrs
APR	10.5%	20.8%	16.1%
FPS	9.8%	20.6%	13.7%
SLY	11.1%	21.1%	16.5%

TABLE II: Table showing the percentage departure of temperature from the magnetic field situation at $r = 4500m$ for different EoS.

Age = 9.7×10^2 yrs, T_e^∞ (observed) = 1.55×10^6 (K) [31, 114]	T_e^∞ (without B field) (K)	T_e^∞ (with B field) (K)
APR	9.006×10^5	1.020×10^6
FPS	1.007×10^6	1.130×10^6
SLY	9.086×10^5	1.018×10^6
Age = 3.3×10^4 yrs, T_e^∞ (observed) = 6.5×10^5 (K) [115, 116]	T_e^∞ (without B field) (K)	T_e^∞ (with B field) (K)
APR	4.300×10^5	5.052×10^5
FPS	5.377×10^5	6.277×10^5
SLY	4.419×10^5	5.171×10^5
Age = 7.3×10^3 yrs, T_e^∞ (observed) = 1×10^6 (K) [117, 118]	T_e^∞ (without B field) (K)	T_e^∞ (with B field) (K)
APR	7.312×10^5	8.409×10^5
FPS	8.494×10^5	9.573×10^5
SLY	7.385×10^5	8.437×10^5

TABLE III: Table showing the comparison of observed surface temperature (T_e^∞) for three NSs with Age = 9.7×10^2 yrs, 3.3×10^4 yrs and 7.3×10^3 yrs, respectively with the theoretically predicted values for different EoS in presence/absence of magnetic field.

In Figure (7a), we have shown the time evolution of the red shifted surface temperature of the NS by incorporating the effect of magnetic field for axion mass ~ 16 meV, assuming that the NS matter satisfies the APR EoS. The variation of temperature in the absence of a magnetic field is also shown for comparison. In the presence of a magnetic field, the temperature versus time curve lies above the corresponding variation curve without the magnetic field for the APR EoS. Between time 10^1 yrs and 10^2 yrs, the separation increases and subsequently, both curves have shown the same qualitative behavior throughout the entire cooling time

duration. However, the temperature in the presence of magnetic field always remain higher than the temperatures without magnetic field at all times. We have shown the comparative behavior of the cooling curves for two other EoSs as well, namely, FPS and SLY, for the same axion mass ~ 16 meV as shown in Figure (7b) and Figure (7c), respectively.

Figure (7b), shows a significant difference in the cooling curves up to 10^2 yrs. The separation decreases beyond 10^5 yrs and the difference in the temperature for the case with magnetic field and without magnetic field be-

comes maximal at $\sim 4 \times 10^1$ yrs. The comparison of the predicted and the observed red shifted surface temperatures for the three NSs are summarized in Table (III). It is worthwhile to mention here that our predicted values of surface temperatures with magnetic field are closer to the corresponding observed values for all three NSs. However, strong sensitivity with respect to the EoS implies that the appropriate fine-tuning is needed in the presence of the magnetic field.

At the early times, the cooling curve shows a significant difference between the results in the presence and absence of magnetic fields. From Figure (7c), it is seen that there is a noteworthy difference between the two curves up to time 10^2 yrs. Subsequently, the separation decreases, and beyond time 10^2 yrs, the difference between the two curves remains almost constant and decreases only at later times.

The EoS of the matter present inside the NS also affects the cooling profile's modification in the presence of magnetic fields. While the overall qualitative features remain the same. There are significant EoS-sensitive departures which indicates that the modeling of neutron stars with strong magnetic fields would have an imprint of the magnetic field distribution. This behavior may affect the observable properties of neutron stars significantly. Finally, we have studied the luminosities of neutrinos, axions, and photons as a function of time in the absence and presence of the magnetic field for three EoSs. We expect to see the imprint of the strong magnetic field in these results.

Figure (8) depicts the luminosity versus time at three different axion masses for APR EoS. The luminosities are all expressed in units of solar luminosity $L_\odot = 3.826 \times 10^{33}$ ergs/s. The photon luminosity [24] at very short times are not accurate as our time unit is coarse and extrapolated. The incomplete modeling of NS due to uncertainty in EoS may also be responsible for the lower estimate of luminosities at short times. The neutrino luminosity dominates over the photon and axion luminosity at early times. The presence of magnetic fields does not change the qualitative behavior, although there is a significant difference in the neutrino luminosity. The magnitude of the luminosity of photons, axions and neutrinos is quite sensitive to the axion mass and also shows a significant departure in the presence of the magnetic field. The time evolution of photon, neutrino and axion luminosities in the absence of magnetic field closely resembles the results in an earlier work [64].

Figure (9) shows the luminosity versus time at three different axion masses for the FPS EoS. The qualitative behavior does not seem to change much with the magnetic field, and a significant departure is seen in the neutrino luminosity and axion luminosity, respectively, in the presence of the magnetic field.

In Figure (10), we have presented the luminosity versus time at three different axion masses for SLY EoS.

Here, also a large departure is seen in the neutrino and axion luminosity, respectively, in the presence of the magnetic field.

IV. CONCLUSION AND FUTURE OUTLOOK

In the present work, our focus is on investigating the variations in luminosity of highly magnetized neutron stars (NSs) in the presence of strong magnetic fields. Additionally, we have also explored the associated cooling rate, characterized by the temperature versus time relationships. Our investigations are based on the assumption that axions, along with neutrinos and photons, constitute the emissions from the core and crust of NSs [90]. Further, we have summarized our findings below:

- The emission characteristics of NSs are subject to intricate influences stemming from factors such as magnetic fields, radiation from nearby objects, and significant gravitational effects from astrophysical entities. Remarkably, the magnetic fields within NSs exert a considerable impact on internal structures, affecting parameters like radius, mass, and pressure profiles. These magnetic fields might even extend their influence to the equation of state (EoS), although their effectiveness under the extreme baryon density conditions within NSs remains uncertain. Nevertheless, the magnetic field distinctly alters thermal and other macroscopic properties.
- While current study did not incorporate the magnetic field's influence on EoSs of core matter, we employed a modified set of Tolman-Oppenheimer-Volkoff (TOV) equations [14] along with three distinct EoSs namely; APR, FPS, and SLY to obtain mass and pressure profiles for NSs. Solving these equations with and without magnetic field terms, the obtained profiles are used to compute cooling rates and luminosities using the NSCool code. This code, incorporating axion emission from the NS core, assumed spherically symmetric NSs with a perfectly isothermal core and excluded heating mechanisms.
- Our analysis encompassed the calculation and plotting of luminosities for neutrinos, axions, and photons, both with and without magnetic fields, considering axion masses of 1 meV, 16 meV, and 30 meV, for each EoS. Notably, the cooling and luminosity data have been plotted with a fixed mean radius, accounting for deformation due to the magnetic field.
- Our findings unequivocally reveal a substantial influence of magnetic fields on NS luminosities and cooling rates. However, it is imperative to acknowledge that this influence is EoS-dependent, and its

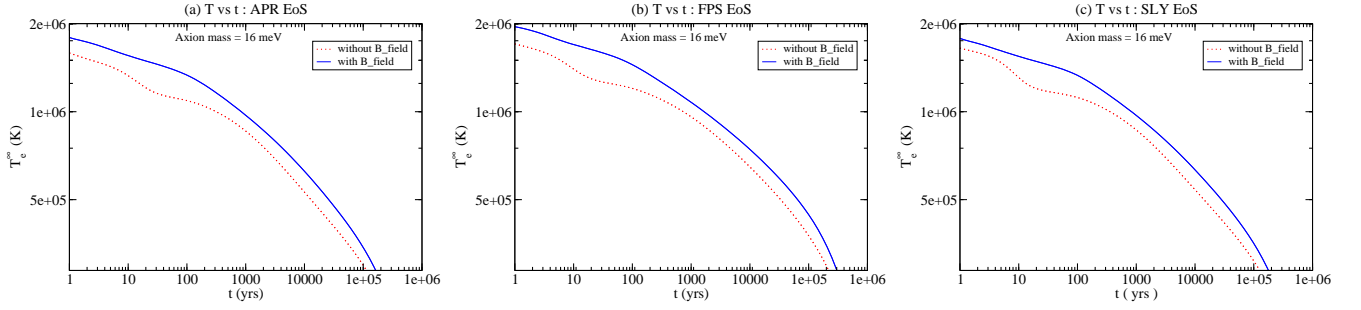


FIG. 7: The variation of temperature with time for three different EoS in the presence and absence of magnetic field.

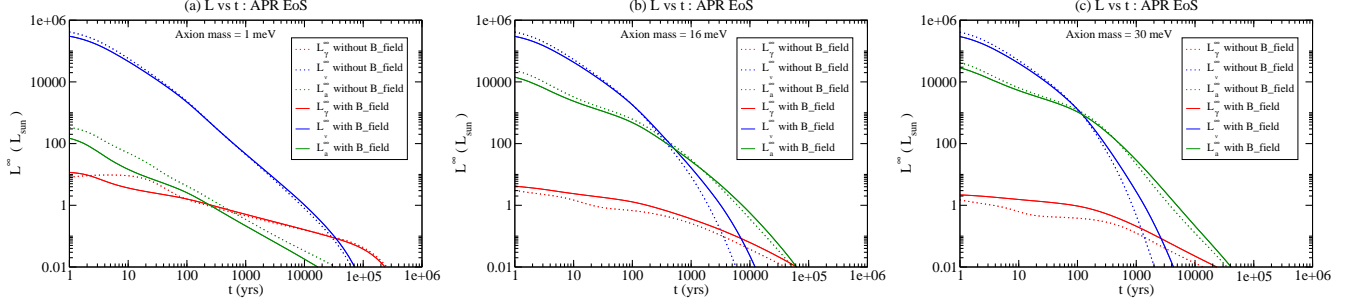


FIG. 8: The variation of luminosity with the time of three different axion masses 1 meV, 16 meV, 30 meV, respectively, for APR EoS in the presence and absence of magnetic field.

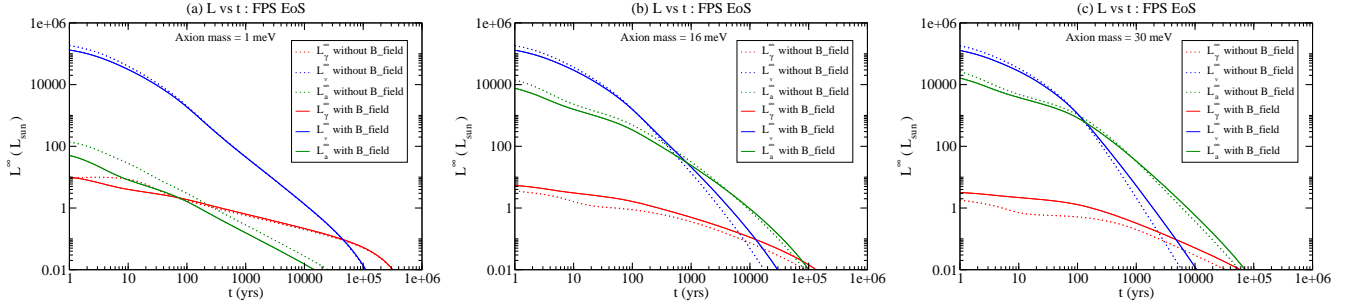


FIG. 9: The variation of luminosity with the time of three different axion masses 1 meV, 16 meV, 30 meV respectively for FPS EoS in the presence and absence of magnetic field.

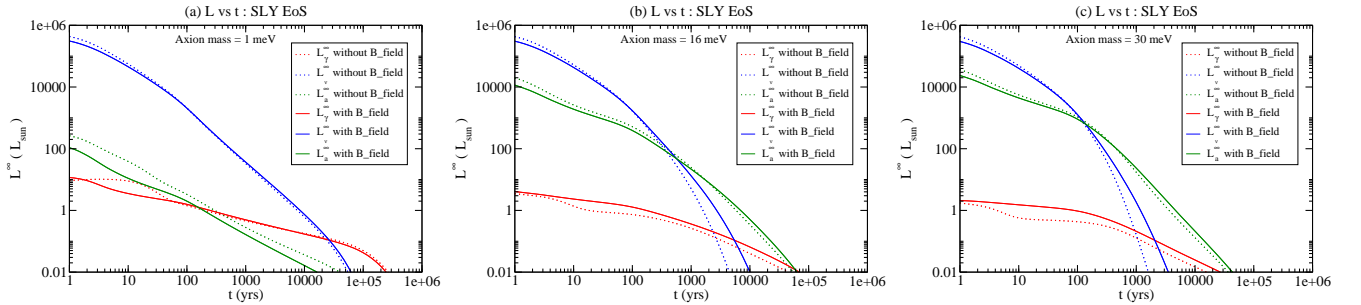


FIG. 10: The variation of luminosity with the time of three different axion masses 1 meV, 16 meV, 30 meV, respectively, for SLY EoS in the presence and absence of magnetic field.

uncertainties are particularly pronounced under extremely high-density and low-temperature conditions. Remarkably, the investigation into axion-to-

photon conversion in these highly magnetized neutron stars remains a subject for future research, as we deferred its exploration in this current study.

Acknowledgments

We are grateful to Dany Page, Malte Buschmann, and T. Opferkuch for clearing our doubts from time to time

while learning to use NSCool code by answering questions. The author (SY) acknowledges Birla Institute of Technology and Science, Pilani, Pilani Campus, Rajasthan, for providing the financial support.

-
- [1] V. M. Kaspi and A. M. Beloborodov, *Annual Review of Astronomy and Astrophysics* **55**, 261 (2017).
 - [2] D. Page and S. Reddy, *Annual Review of Nuclear and Particle Science* **56**, 327 (2006).
 - [3] D. Page, J. M. Lattimer, M. Prakash, and A. W. Steiner, *The Astrophysical Journal Supplement Series* **155**, 623 (2004).
 - [4] D. Page, U. Geppert, and F. Weber, *Nuclear Physics A* **777**, 497 (2006), special Issue on Nuclear Astrophysics.
 - [5] D. Page, p. 183 (1998).
 - [6] A. Dohi, R. Kase, R. Kimura, K. Yamamoto, and M.-a. Hashimoto, *Progress of Theoretical and Experimental Physics* **2021** (2021), 093E01.
 - [7] A. Potekhin, A. I. Chugunov, and G. Chabrier, *aap* **629**, A88 (2019).
 - [8] A. Y. Potekhin, *Phys. Usp.* **57**, 735 (2014), 1403.0074.
 - [9] M. V. Beznogov, D. Page, and E. Ramirez-Ruiz, *apj* **888**, 97 (2020).
 - [10] D. Yakovlev, K. Levenfish, and P. Haensel, *aap* **407**, 265 (2003).
 - [11] M. V. Beznogov, E. Rrapaj, D. Page, and S. Reddy, *Phys. Rev. C* **98**, 035802 (2018).
 - [12] V. Dexheimer, B. Franzon, R. O. Gomes, R. L. S. Farias, S. S. Avancini, and S. Schramm, *Astron. Nachr.* **338**, 1052 (2017).
 - [13] V. Dexheimer, B. Franzon, R. Gomes, R. Farias, S. Avancini, and S. Schramm, *Physics Letters B* **773**, 487 (2017).
 - [14] D. Chatterjee and M. Novak, *Jerome Oertel, prc* **99**, 055811 (2019).
 - [15] M. Beznogov and D. Yakovlev, *mnras* **447**, 1598 (2015).
 - [16] V. Dexheimer, R. Negreiros, and S. Schramm, *The European Physical Journal A* **48**, 1 (2012).
 - [17] G. E. Brown, K. Kubodera, D. Page, and P. Pizzochero, *Phys. Rev. D* **37**, 2042 (1988).
 - [18] D. Yakovlev and C. Pethick, *Annual Review of Astronomy and Astrophysics* **42**, 169 (2004).
 - [19] M. V. Beznogov, J. Novak, D. Page, and A. R. Raduta, *The Astrophysical Journal* **942**, 72 (2023).
 - [20] A. Potekhin and G. Chabrier, *aap* **538**, A115 (2012).
 - [21] R. O. Gomes, B. Franzon, V. Dexheimer, and S. Schramm, *The Astrophysical Journal* **850**, 20 (2017).
 - [22] D. Yakovlev, O. Gnedin, M. Gusakov, A. Kaminker, K. Levenfish, and A. Potekhin, *Nuclear Physics A* **752**, 590 (2005).
 - [23] D. Yakovlev, O. Gnedin, A. Kaminker, K. Levenfish, and A. Potekhin, *Advances in Space Research* **33**, 523 (2004).
 - [24] A. Y. Potekhin, J. A. Pons, and D. Page, *ssr* **191**, 239 (2015).
 - [25] A. Y. Potekhin and G. Chabrier, *A&A* **609**, A74 (2018).
 - [26] P. G. Jonker, D. Steeghs, D. Chakrabarty, and A. M. Juett, *The Astrophysical Journal* **665**, L147 (2007).
 - [27] M. Sinha, B. Mukhopadhyay, and A. Sedrakian, *Nuclear Physics A* **898**, 43 (2013).
 - [28] L. Lopes and D. Menezes, *Journal of Cosmology and Astroparticle Physics* **2015**, 002 (2015).
 - [29] V. Gomes, R. O. Dexheimer and C. A. Z. Vasconcellos, *arXiv e-prints* (2013).
 - [30] D. Chatterjee, T. Elghozi, J. Novak, and M. Oertel, *Monthly Notices of the Royal Astronomical Society* **447**, 3785 (2015).
 - [31] U. Geppert, M. Kuker, and D. Page, *A&A* **426**, 267 (2004).
 - [32] A. Sedrakian, *Prog. Part. Nucl. Phys.* **58**, 168 (2007), nucl-th/0601086.
 - [33] A. D. Kaminker, D. G. Yakovlev, A. Y. Potekhin, N. Shibasaki, P. S. Shternin, and O. Y. Gnedin, *Monthly Notices of the Royal Astronomical Society* **371**, 477 (2006).
 - [34] S. Reddy and D. Zhou, *Phys. Rev. D* **105**, 023026 (2022), 2107.06279.
 - [35] M. Bocquet, S. Bonazzola, E.ourgoulhon, and J. Novak, *aap* **301**, 757 (1995), gr-qc/9503044.
 - [36] M. Bhattacharya, B. Mukhopadhyay, and S. Mukerjee, *Monthly Notices of the Royal Astronomical Society* **477**, 2705 (2018).
 - [37] D. D. Ofengeim and D. G. Yakovlev, *Monthly Notices of the Royal Astronomical Society* **467**, 3598 (2017).
 - [38] M. Prakash, I. Bombaci, M. Prakash, P. J. Ellis, J. M. Lattimer, and R. Knorren, *Physics Reports* **280**, 1 (1997).
 - [39] J. M. Lattimer and M. Prakash, *The Astrophysical Journal* **550**, 426 (2001).
 - [40] K. H. Prendergast, *Astrophys. J.* **123**, 498 (1956).
 - [41] J. N. Braithwaite, *aap* **450**, 1077 (2006).
 - [42] J. Braithwaite, *Monthly Notices of the Royal Astronomical Society* **397**, 763 (2009).
 - [43] J. Braithwaite and H. C. Spruit, *Nature (London)* **431**, 819 (2004).
 - [44] A. Y. Potekhin, D. A. Zyuzin, D. G. Yakovlev, M. V. Beznogov, and Y. A. Shibano, *Monthly Notices of the Royal Astronomical Society* **496**, 5052 (2020).
 - [45] D. Page, *ascl:1609.009* (2016), 1609.009.
 - [46] R. C. Tolman, *Phys. Rev.* **55**, 364 (1939).
 - [47] J. R. Oppenheimer and G. M. Volkoff, *Phys. Rev.* **55**, 374 (1939).
 - [48] J. B. Hartle and K. S. Thorne, *Astrophys. J.* **153**, 807 (1968).
 - [49] M. L. Pattersons and A. Sulaksono, *European Physical Journal C* **81**, 698 (2021).
 - [50] D. Psaltis and F. Özel, *The Astrophysical Journal* **792**, 87 (2014).
 - [51] M. E. Gusakov, A. D. Kaminker, D. G. Yakovlev, and O. Y. Gnedin, *Monthly Notices of the Royal Astronomical Society* **363**, 555 (2005).
 - [52] A. Akmal, V. R. Pandharipande, and D. G. Ravenhall, *Phys. Rev. C* **58**, 1804 (1998).
 - [53] P. Haensel, J. L. Zdunik, and F. Douchin, *Astronomy & Astrophysics* **385**, 301 (2002).

- [54] A. S. Schneider, C. Constantinou, B. Muccioli, and M. Prakash, *Physical Review C* **100** (2019).
- [55] A. Broderick, M. Prakash, and J. M. Lattimer, *The Astrophysical Journal* **537**, 351 (2000).
- [56] E. Flowers, M. Ruderman, and P. Sutherland, *Astrophys. J.* **205**, 541 (1976).
- [57] R. Wijnands, N. Degenaar, and D. Page, *Journal of Astrophysics and Astronomy* **38**, 1 (2017).
- [58] M. Prakash, *Physics Reports* **242**, 297 (1994).
- [59] N. Iwamoto, L. Qin, M. Fukugita, and S. Tsuruta, *Phys. Rev. D* **51**, 348 (1995).
- [60] N. Iwamoto, *Phys. Rev. Lett.* **44**, 1637 (1980).
- [61] D. Page, M. Prakash, J. M. Lattimer, and A. W. Steiner, *Phys. Rev. Lett.* **106**, 081101 (2011).
- [62] E. F. Brown, A. Cumming, F. J. Fattoyev, C. J. Horowitz, D. Page, and S. Reddy, *Phys. Rev. Lett.* **120**, 182701 (2018).
- [63] C. O. Heinke, P. G. Jonker, R. Wijnands, C. J. Deloye, and R. E. Taam, *The Astrophysical Journal* **691**, 1035 (2009).
- [64] M. Buschmann, C. Dessert, J. W. Foster, A. J. Long, and B. R. Safdi, *Phys. Rev. Lett.* **128**, 091102 (2022).
- [65] A. Y. Potekhin, D. G. Yakovlev, G. Chabrier, and O. Y. Gnedin, *The Astrophysical Journal* **594**, 404 (2003).
- [66] E. H. Gudmundsson, C. J. Pethick, and R. I. Epstein, *apj* **272**, 286 (1983).
- [67] K. Nomoto and S. Tsuruta, *apj* **312**, 711 (1987).
- [68] A. Y. Potekhin, G. Chabrier, and D. G. Yakovlev, *aap* **323**, 415 (1997).
- [69] A. Y. Potekhin and D. G. Yakovlev, *A&A* **374**, 213 (2001).
- [70] A. Y. Potekhin, G. Chabrier, and D. G. Yakovlev, pp. 353–361 (2007).
- [71] A. Y. Potekhin, V. Urpin, and G. Chabrier, *A&A* **443**, 1025 (2005).
- [72] M. Beznogov, A. Potekhin, and D. Yakovlev, *mnras* **459**, 1569 (2016).
- [73] A. D. Kaminker, A. A. Kaurov, A. Y. Potekhin, and D. G. Yakovlev, *Monthly Notices of the Royal Astronomical Society* **442**, 3484 (2014).
- [74] M. Beznogov, A. Potekhin, and D. Yakovlev, *Physics Reports* **919**, 1 (2021), heat blanketing envelopes of neutron stars.
- [75] A. I. Chugunov and P. Haensel, *Monthly Notices of the Royal Astronomical Society* **381**, 1143 (2007), ISSN 0035-8711.
- [76] R. D. Peccei and H. R. Quinn, *Phys. Rev. Lett.* **38**, 1440 (1977).
- [77] R. D. Peccei and H. R. Quinn, *Phys. Rev. D* **16**, 1791 (1977).
- [78] S. Weinberg, *Phys. Rev. Lett.* **40**, 223 (1978).
- [79] F. Wilczek, *Phys. Rev. Lett.* **40**, 279 (1978).
- [80] Z. Bogorad, A. Hook, Y. Kahn, and Y. Soreq, *Phys. Rev. Lett.* **123**, 021801 (2019).
- [81] H. Umeda, N. Iwamoto, S. Tsuruta, L. Qin, and K. Nomoto, *arXiv preprint astro-ph/9806337* (1998).
- [82] L. Abbott and P. Sikivie, *Physics Letters B* **120**, 133 (1983).
- [83] R. L. Davis, *Phys. Rev. D* **32**, 3172 (1985).
- [84] C. Dessert, A. J. Long, and B. R. Safdi, *Physical Review Letters* **128** (2022).
- [85] J. Preskill, M. B. Wise, and F. Wilczek, *Physics Letters B* **120**, 127 (1983).
- [86] M. Dine and W. Fischler, *Physics Letters B* **120**, 137 (1983).
- [87] M. Buschmann, J. W. Foster, and B. R. Safdi, *Phys. Rev. Lett.* **124**, 161103 (2020).
- [88] F. Chadha-Day, J. Ellis, and D. J. Marsh, *Science advances* **8**, eabj3618 (2022).
- [89] C. Adams, N. Aggarwal, A. Agrawal, R. Balafendiev, C. Bartram, M. Baryakhtar, H. Bekker, P. Belov, K. Berggren, A. Berlin, et al. (2022).
- [90] M. Buschmann, R. T. Co, C. Dessert, and B. R. Safdi, *Phys. Rev. Lett.* **126**, 021102 (2021).
- [91] L. D. Duffy and K. van Bibber, *New Journal of Physics* **11**, 105008 (2009).
- [92] M. D. Marsh, H. R. Russell, A. C. Fabian, B. R. McNamara, P. Nulsen, and C. S. Reynolds, *Journal of Cosmology and Astroparticle Physics* **2017**, 036 (2017).
- [93] C. Dessert, A. J. Long, and B. R. Safdi, *Phys. Rev. Lett.* **123**, 061104 (2019).
- [94] S. Chaudhuri, P. W. Graham, K. Irwin, J. Mardon, S. Rajendran, and Y. Zhao, *Phys. Rev. D* **92**, 075012 (2015).
- [95] M. S. Pshirkov and S. B. Popov, *Journal of Experimental and Theoretical Physics* **108**, 384 (2009).
- [96] N. Du, N. Force, R. Khatriwada, E. Lentz, R. Ottens, L. J. Rosenberg, G. Rybka, G. Carosi, N. Woollett, D. Bowring, et al. (ADMX Collaboration), *Phys. Rev. Lett.* **120**, 151301 (2018).
- [97] Y. Kahn, B. R. Safdi, and J. Thaler, *Phys. Rev. Lett.* **117**, 141801 (2016).
- [98] J. W. Foster, N. L. Rodd, and B. R. Safdi, *Phys. Rev. D* **97**, 123006 (2018).
- [99] A. Sedrakian, *Physical Review D* **93** (2016).
- [100] L. B. Leinson, *Journal of Cosmology and Astroparticle Physics* **2019**, 031 (2019).
- [101] D. Page, U. Geppert, and F. Weber, *Nucl. Phys. A* **777**, 497 (2006), astro-ph/0508056.
- [102] D. Page, J. M. Lattimer, M. Prakash, and A. W. Steiner, *The Astrophysical Journal* **707**, 1131 (2009).
- [103] L. Leinson, *Physics Letters B* **473**, 318 (2000).
- [104] J. Keller and A. Sedrakian, *Nuclear Physics A* **897**, 62 (2013).
- [105] U. Geppert, M. Küker, and D. Page, *Astronomy & Astrophysics* **457**, 937 (2006).
- [106] E. E. Kolomeitsev and D. N. Voskresensky, *Physical Review C* **77** (2008).
- [107] J. M. Lattimer, C. J. Pethick, M. Prakash, and P. Haensel, *Phys. Rev. Lett.* **66**, 2701 (1991).
- [108] A. Yakovlev, D. G. Kaminker, O. Gnedin, and P. Haensel, *Phys. Rep.* **354**, 1 (2001).
- [109] N. Iwamoto, *Phys. Rev. Lett.* **53**, 1198 (1984).
- [110] D. E. Morris, *Phys. Rev. D* **34**, 843 (1986).
- [111] G. Raffelt and L. Stodolsky, *Phys. Rev. D* **37**, 1237 (1988).
- [112] D. G. Yakovlev, A. D. Kaminker, and K. P. Levenfish, *343*, 650 (1999).
- [113] A. D. Kaminker, P. Haensel, and D. G. Yakovlev, **345**, L14 (1999).
- [114] J. A. O’Dea, F. A. Jenet, T.-H. Cheng, C. M. Buu, M. Beroiz, S. W. Asmar, and J. W. Armstrong, *The Astronomical Journal* **147**, 100 (2014).
- [115] F. Xu, J.-J. Geng, X. Wang, L. Li, and Y.-F. Huang, *Monthly Notices of the Royal Astronomical Society* **509**, 4916 (2021).
- [116] C.-Y. Ng, R. W. Romani, W. F. Briskin, S. Chatterjee, and M. Kramer, *The Astrophysical Journal* **654**, 487 (2007).

- (2007).
- [117] V. E. Zavlin, The Astrophysical Journal **665**, L143 (2007).
- [118] A. Kirichenko, A. Danilenko, R. E. Mennickent, G. Pavlov, Y. Shibano, S. Zharikov, and D. Zyuzin (2012).